Electronic Supplementary Material (ESI) for Inorganic Chemistry Frontiers.

Supplementary information

Layered Double Hydroxide Derived Bimetallic Nickel-Iron Selenide as an Active Electrocatalyst for Nitrogen Fixation under Ambient Conditions

Shiyu Yang,[a] Wen Ye,[c] Demei Zhang[a], Xiaoyu Fang[a] and Dongpeng Yan*[abd]

a. Beijing Key Laboratory of Energy Conversion and Storage Materials, College of Chemistry Beijing Normal University, Beijing 100875, P. R. China. E-mail: yandp@bnu.edu.cn
b. College of Chemistry, Key Laboratory of Radiopharmaceuticals, Ministry of Education, Beijing Normal University, Beijing 100875, P. R. China.
c. School of Chemistry and Biological Engineering, Basic Experimental Center For Natural Science, University of Science and Technology Beijing, Beijing 100083, P. R. China
d. College of Chemistry and Molecular Engineering, Zhengzhou University, Zhengzhou 450001, China

Experimental details

Chemicals

All chemical reagents were directly used without any further purification. Nickel(II) nitrate hexahydrate ($Ni(NO_3)_2.6H_2O$), iron(III) nitrate nonahydrate ($Fe(NO_3)_3.9H_2O$), triethanolamine ($N(CH_2CH_2OH)_3$), triethanolamine (TEA), selenium powder (Se), ammonium iron(II) sulfate ($Fe(NH_4)_2{\cdot}(SO_4)_2{\cdot}6H_2O$), citric acid (CA), ethyl alcohol (C_2H_5OH), salicylic acid ($C_7H_6O_3$), sodium citrate dihydrate ($C_6H_5Na_3O_7{\cdot}2H_2O$), sodium nitroferricyanide dihydrate ($C_5FeN_6Na_2O{\cdot}2H_2O$), sodium hypochlorite solution (NaClO), p-dimethylaminobenzaldehyde ($C_9H_{11}NO$), hydrazine dihydrochloride ($N_2H_4{\cdot}HCl$), sodium sulfate (Na_2SO_4), potassium sulfate (K_2SO_4), lithium sulphat (Li_2SO_4), carbon paper (C), 5% Nafion solution, iso-propyl alcohol ($(CH_3)_2CHOH$), 211 Nafion membrane, deionized water, N_2 gas (99.99%), Ar gas (99.99%), $^{15}N_2$ gas (98%).

Characterization.

The morphology, microstructure and chemical composition of the samples are characterized by field emission scanning electron microscopy (FESEM, Hitachi S-8010), pH meter (METTLER TOLEDO), transmission electron microscopy (TEM, JEOL, JEM-2100F), X-ray diffraction (XRD, Rigaku Ultima-IV), and X-ray photoelectron spectroscopy (XPS, Thermo VG ESCALAB MK II).

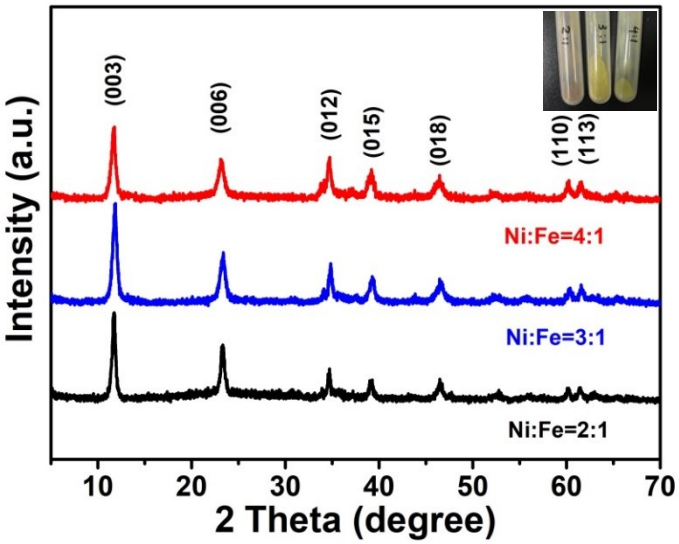

Figure S1. XRD image of NiFe-LDH.

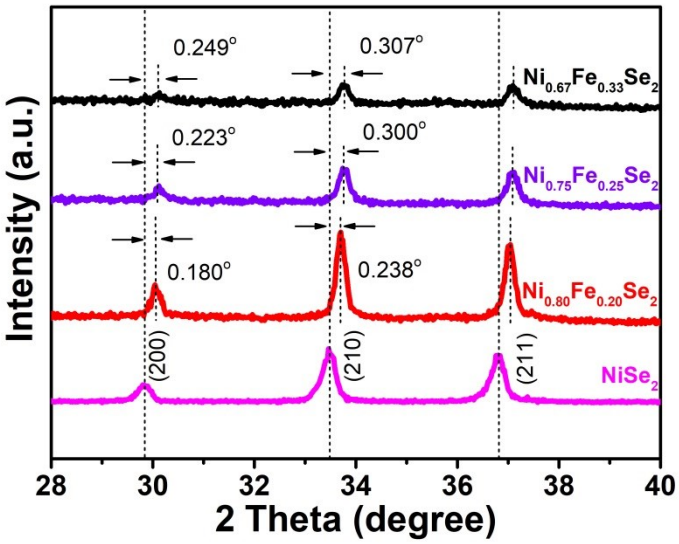

Figure S2. The local enlarged XRD patterns of $Ni_{0.67}Fe_{0.33}Se_2$, $Ni_{0.75}Fe_{0.25}Se_2$ and $Ni_{0.80}Fe_{0.20}Se_2$.

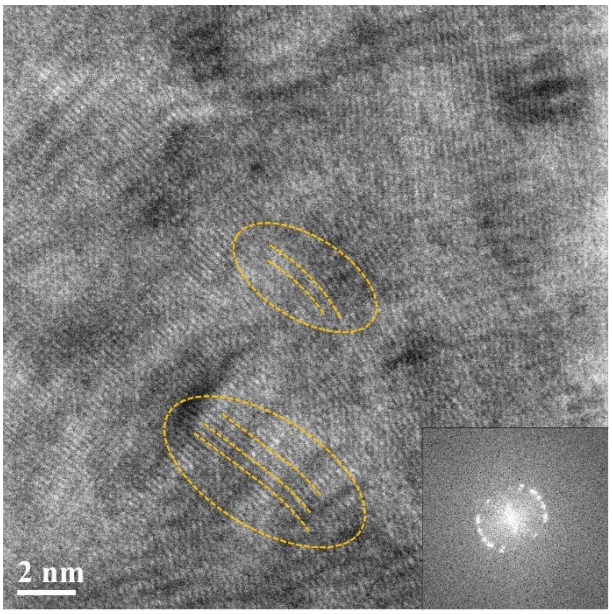

Figure S3. The HRTEM images and FFT patterns of $Ni_{0.75}Fe_{0.25}Se_2$

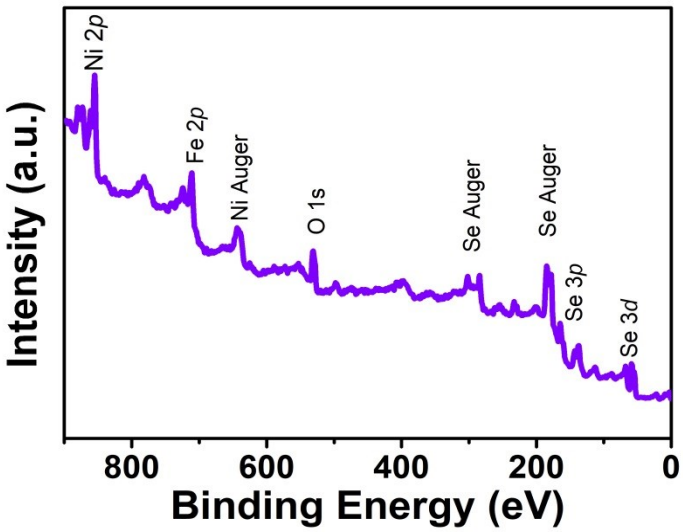

Figure S4. XPS survey scan spectrum of the $Ni_{0.75}Fe_{0.25}Se_2$ catalyst.

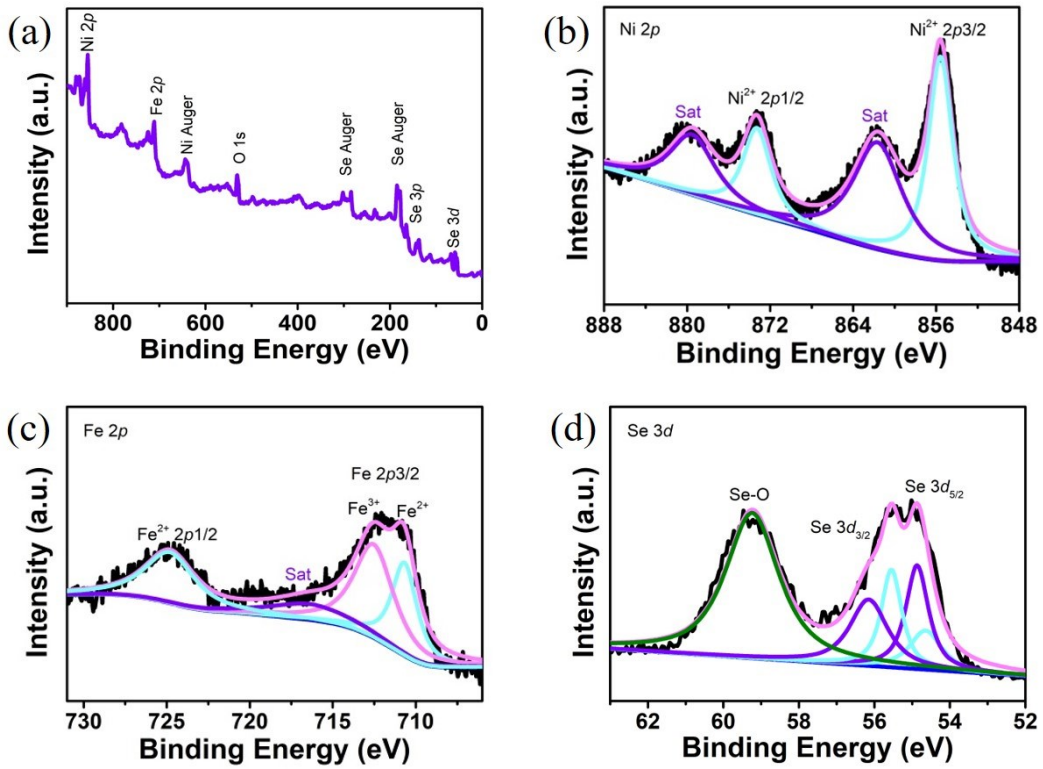

Figure S5. (a) XPS spectra of $Ni_{0.67}Fe_{0.33}Se_2$. (b) Ni 2p; (c) Fe 2p; and (d) Se 3d.

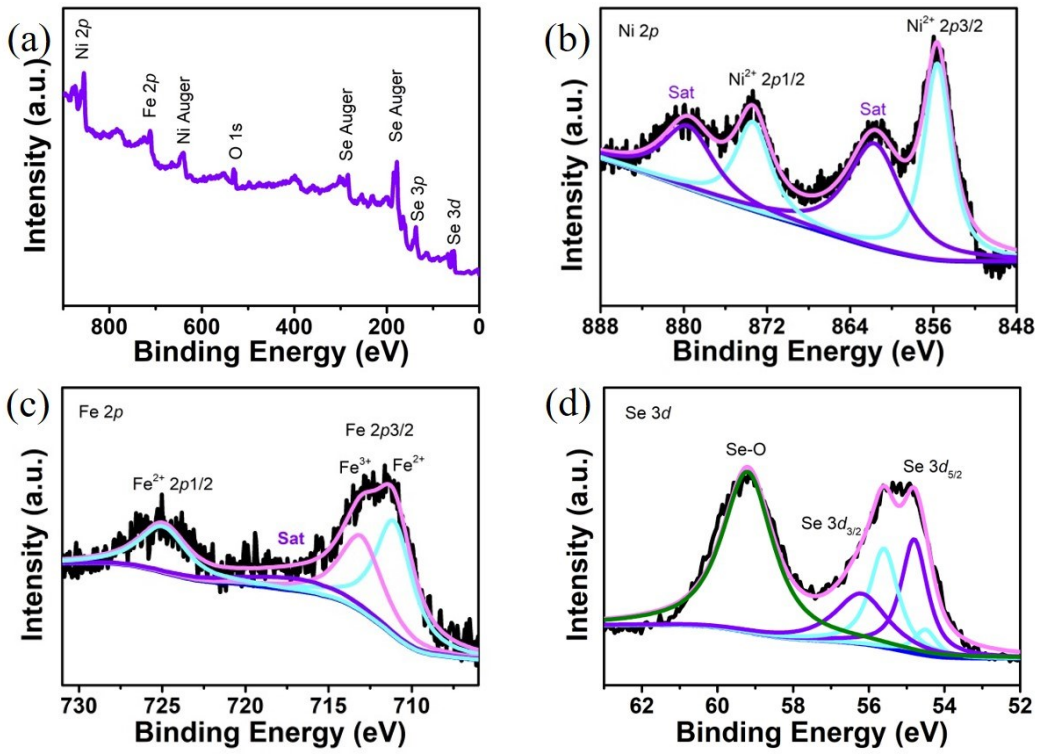

Figure S6. (a) XPS spectra of $Ni_{0.80}Fe_{0.20}Se_2$. (b) Ni 2p; (c) Fe 2p; and (d) Se 3d.

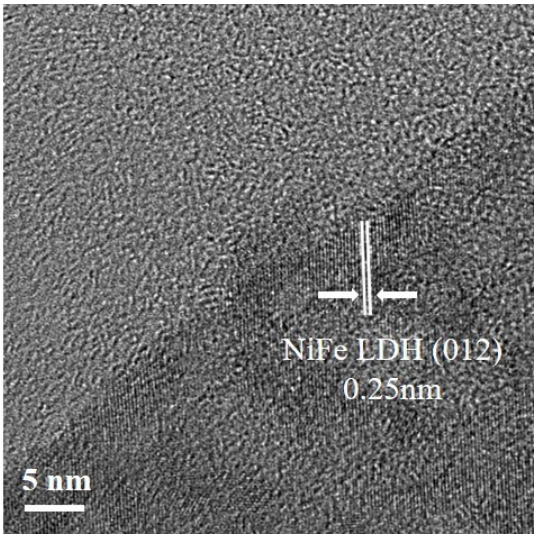

Figure S7. The HRTEM image of $Ni_{0.75}Fe_{0.25}$-LDH.

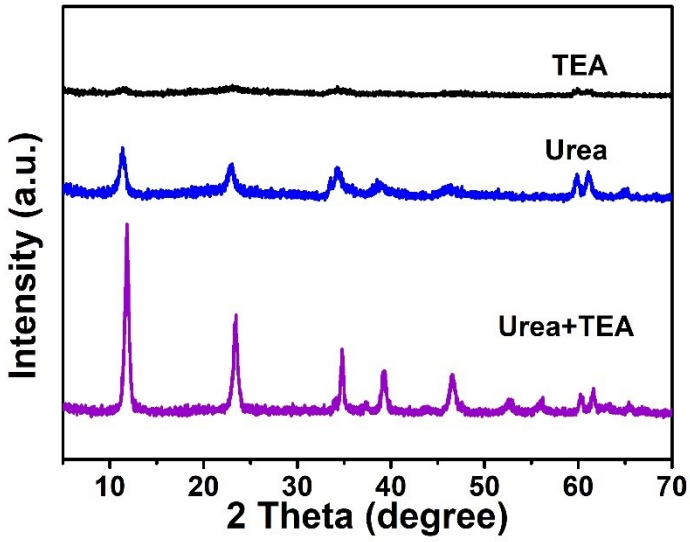

Figure S8. XRD image of NiFe-LDH with different basic materials.

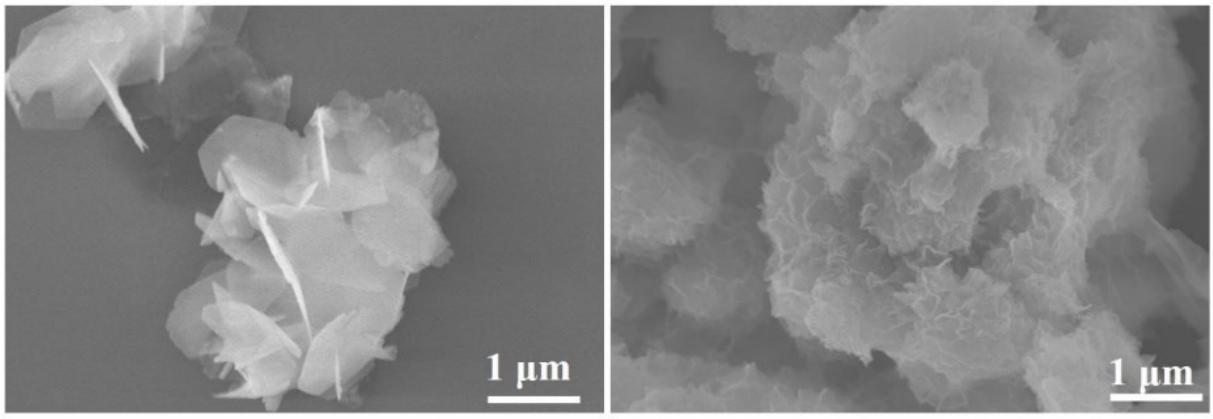

Figure S9. SEM images of $Ni_{0.75}Fe_{0.25}$-LDH.

(The left with urea and TEA addition, the right with urea only.)

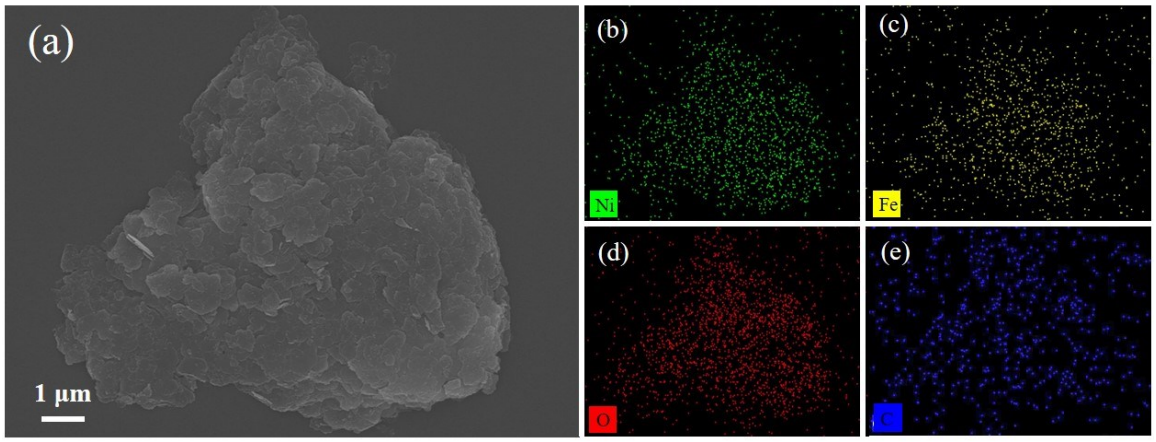

Figure S10. (a) SEM images and (b-e) EDS elemental mapping images of $Ni_{0.67}Fe_{0.33}$-LDH for Ni (green), Fe (golden), O (red) and C (purple).

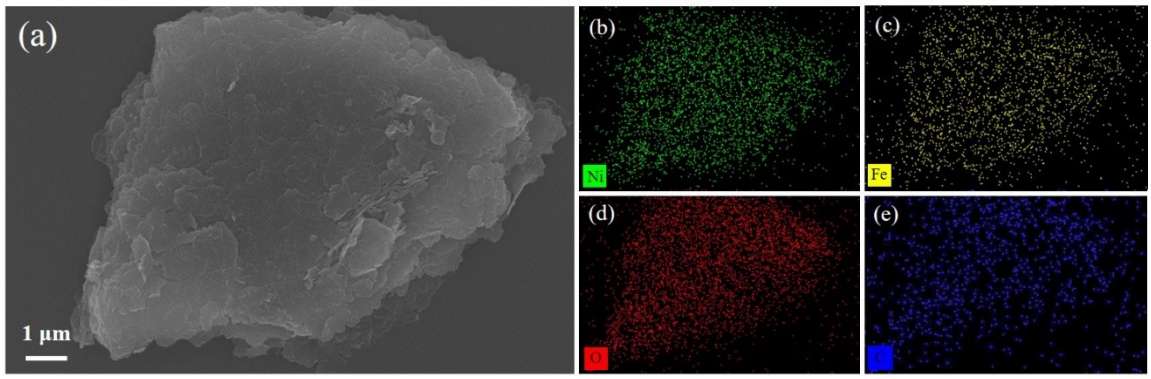

Figure S11. (a) SEM images and (b-e) EDS elemental mapping images of $Ni_{0.75}Fe_{0.25}$-LDH. for Ni (green), Fe (golden), O (red) and C (purple).

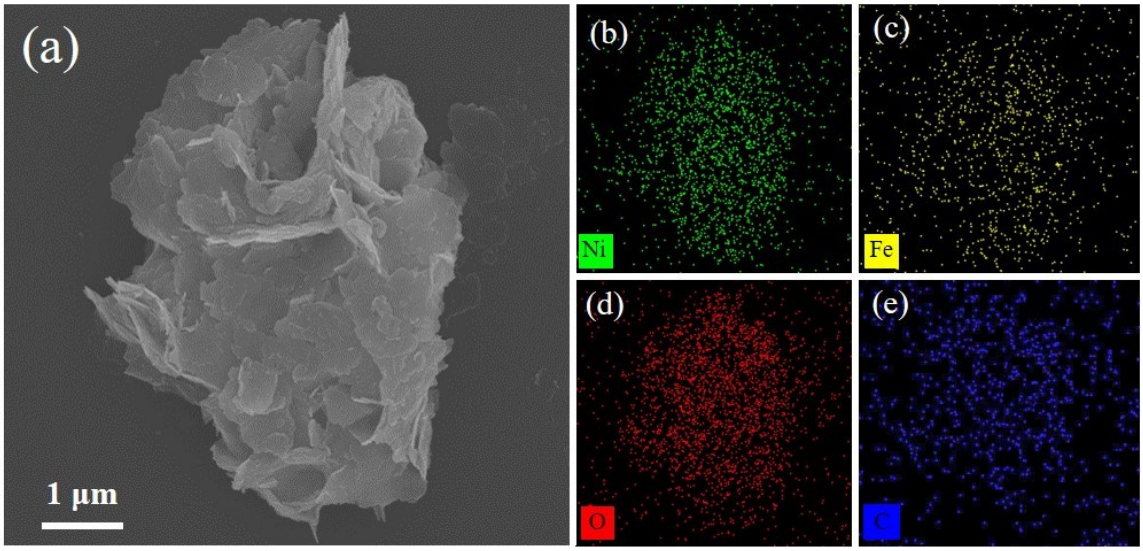

Figure S12. (a) SEM images and (b-e) EDS elemental mapping images of $Ni_{0.80}Fe_{0.20}$-LDH. for Ni (green), Fe (golden), O (red) and C (purple).

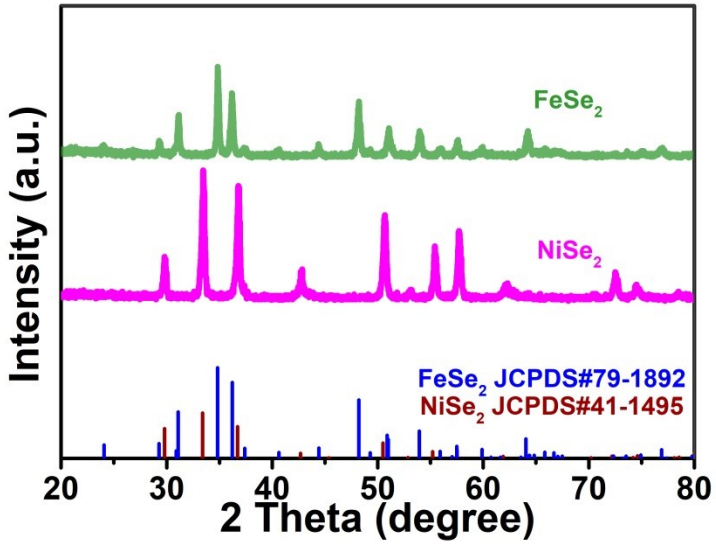

Figure S13. The XRD image of $FeSe_2$ and $NiSe_2$.

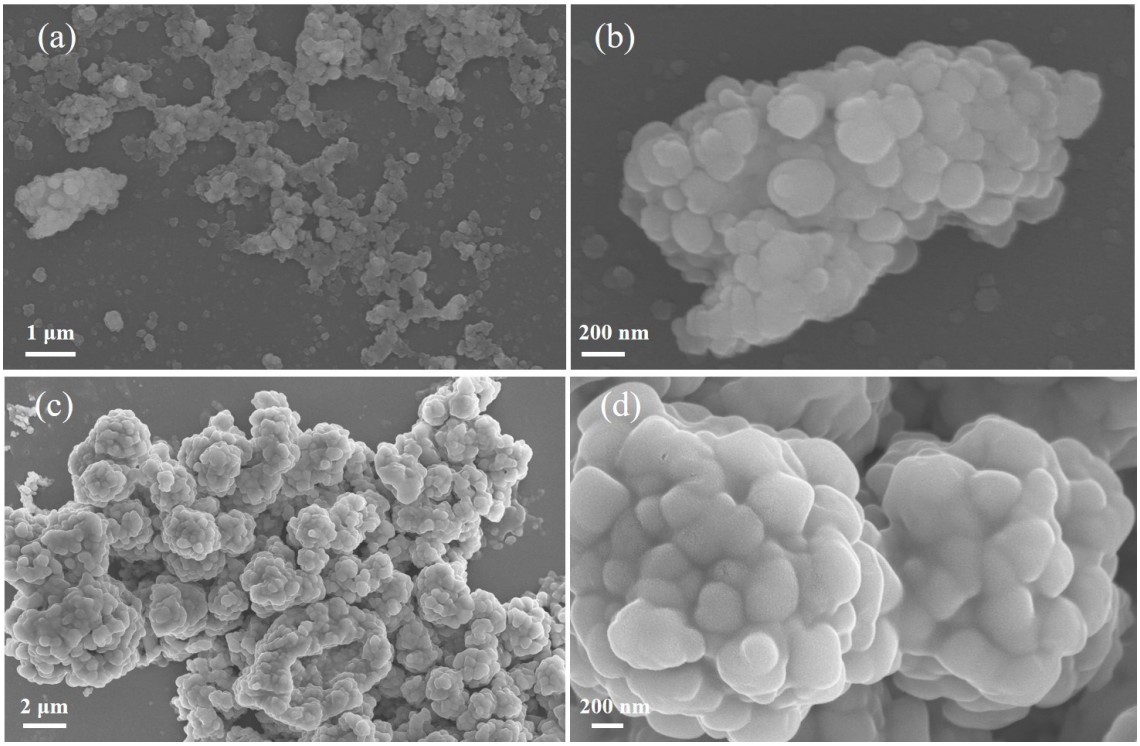

Figure S14. (a-b) low- and high-magnification SEM images of $NiSe_2$.

(c-d) low- and high-magnification SEM images of $FeSe_2$.

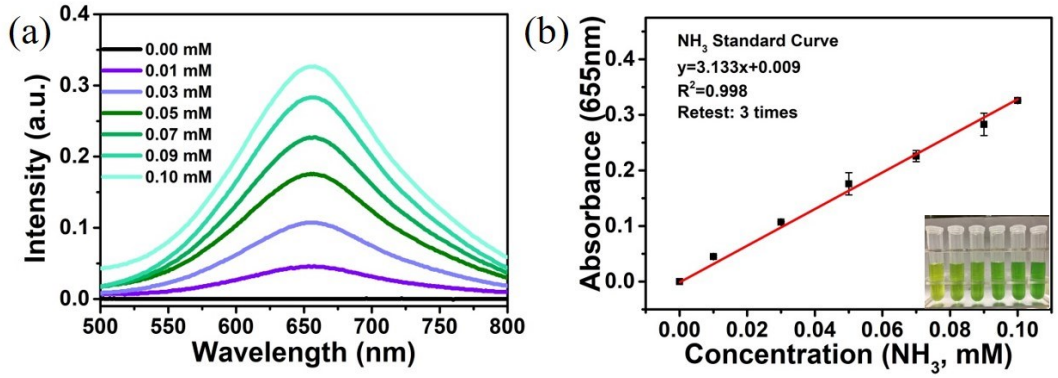

Figure S15. (a) UV–Vis absorption spectra of various NH_3 concentrations after incubated for 2 h in 0.1 M Li_2SO_4 aqueous solution at room temperature. (b) Calibration curve used for calculation of NH_3 concentrations.

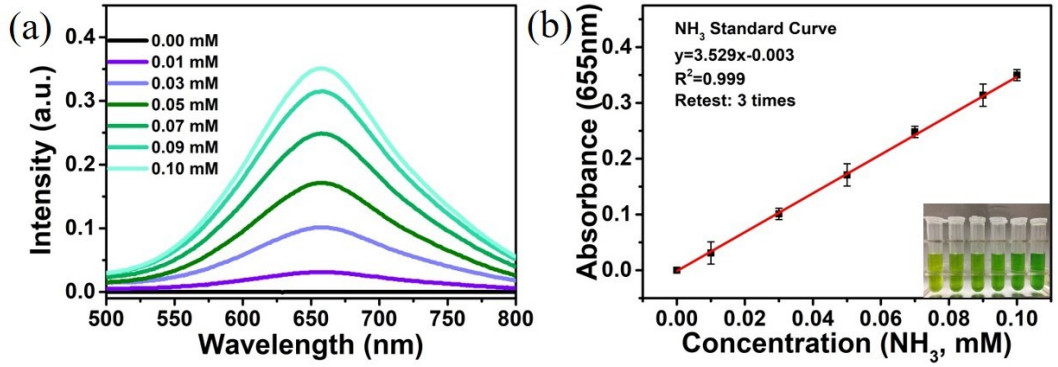

Figure S16. (a) UV–Vis absorption spectra of various NH_3 concentrations after incubated for 2 h in 0.1 M Na_2SO_4 aqueous solution at room temperature. (b) Calibration curve used for calculation of NH_3 concentrations.

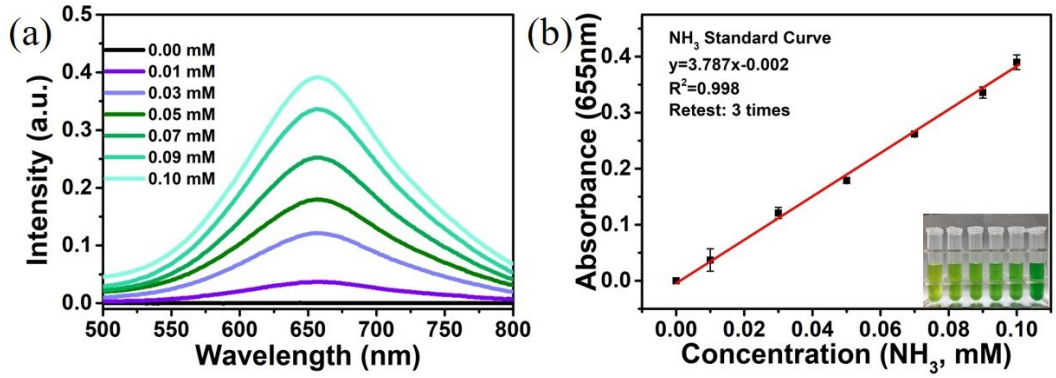

Figure S17. (a) UV–Vis absorption spectra of various NH_3 concentrations after incubated for 2 h in 0.1 M K_2SO_4 aqueous solution at room temperature. (b) Calibration curve used for calculation of NH_3 concentrations.

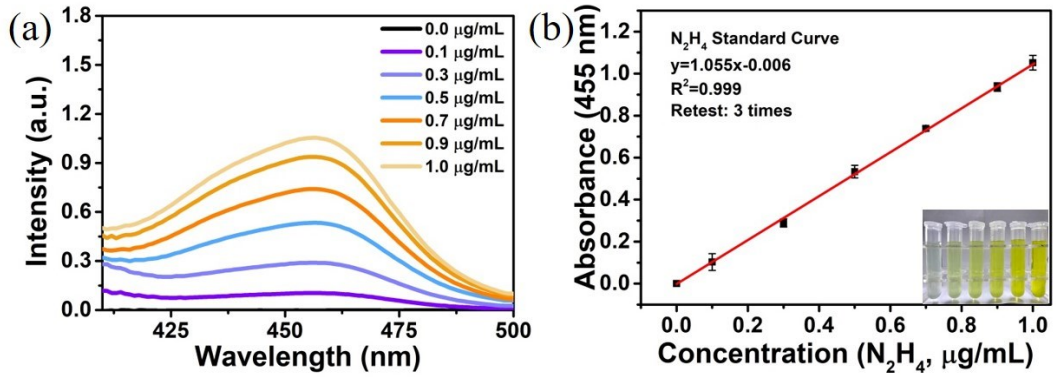

Figure S18. (a) UV–Vis absorption spectra of various N_2H_4 concentrations after incubated for 20 min in 0.1 M Li_2SO_4 aqueous solution at room temperature. (b) Calibration curve used for calculation of N_2H_4 concentrations.

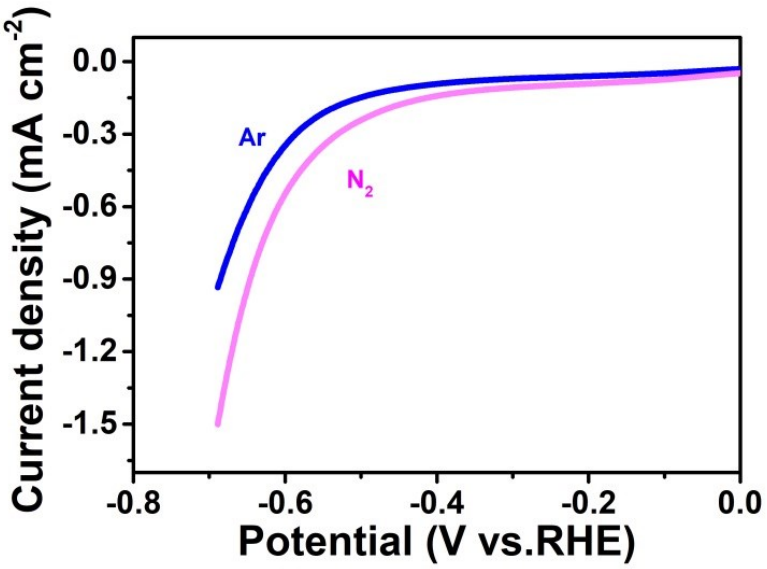

Figure S19. LSV curves of $Ni_{0.75}Fe_{0.25}Se_2$ sample in the N_2-saturated and Ar-saturated 0.1 M Li_2SO_4 aqueous solution, respectively.

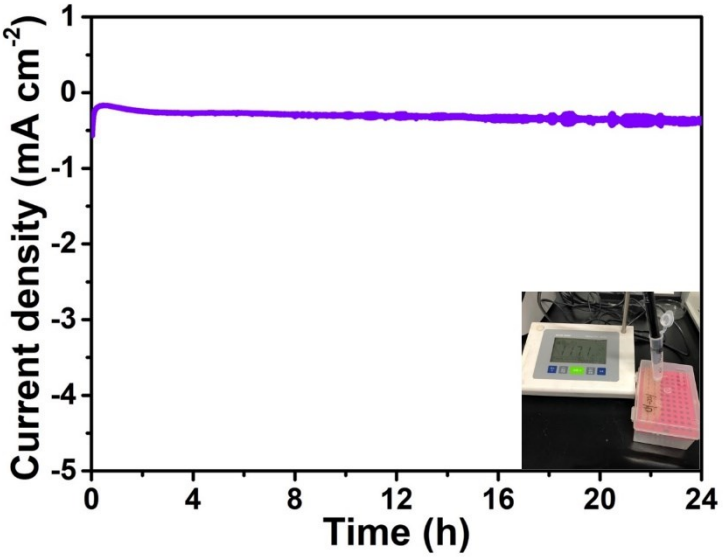

Figure S20. Chrono-amperometry results of $Ni_{0.75}Fe_{0.25}$-LDH for stability test (insert is the pH reading after 24h reaction).

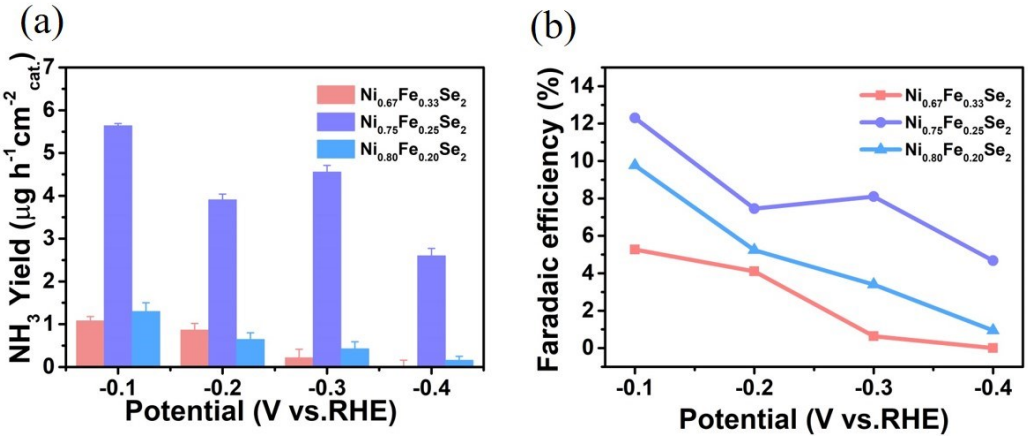

Figure S21. Electrocatalytic NRR of $Ni_{0.67}Fe_{0.33}Se_2$, $Ni_{0.75}Fe_{0.25}Se_2$ and $Ni_{0.80}Fe_{0.20}Se_2$ at ambient conditions. (a) Yield rate of NH_3 and (b) Faradaic efficiency at each given potential.

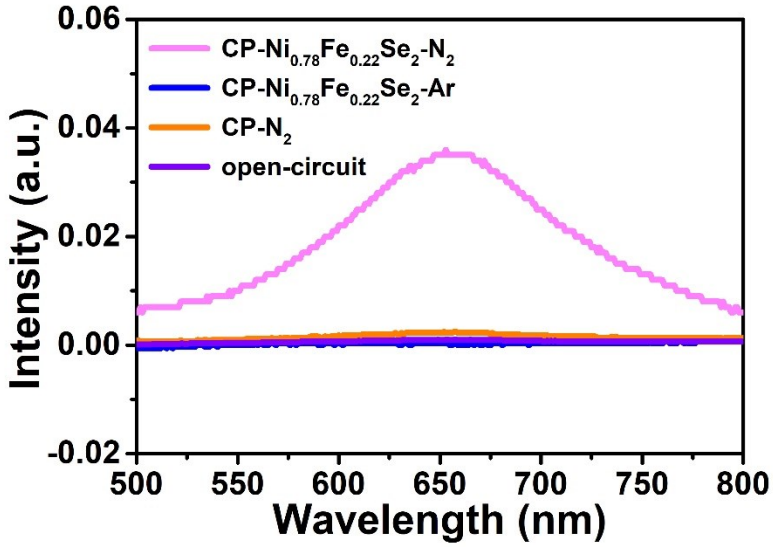

Figure S22. UV-Vis absorption spectra of the electrolyte stained with indophenol indicator in four different condition at -0.1 V *vs*. RHE.

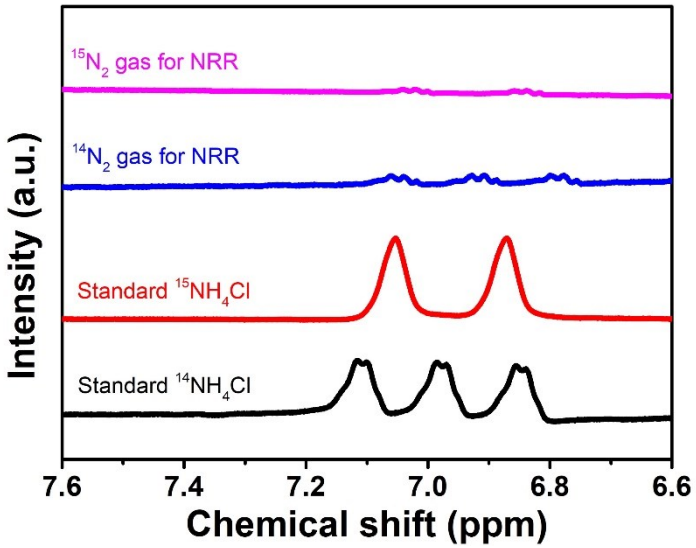

Figure S23. 1H NMR spectra of standard $^{14}NH_4Cl$ and $^{15}NH_4Cl$ solution, also the Li_2SO_4 electrolyte fed by $^{14}N_2$ and $^{15}N_2$ after the electrolytic reaction.

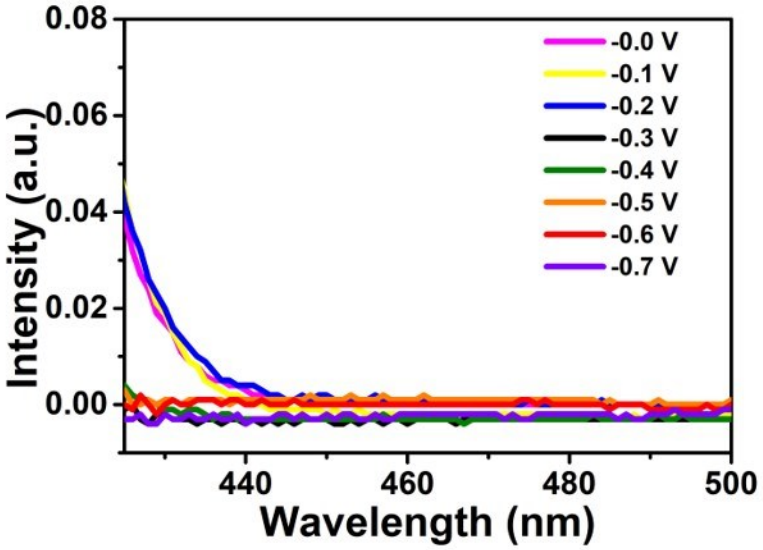

Figure S24. UV-Vis absorbance curves of $Ni_{0.75}Fe_{0.25}Se_2$ in Li_2SO_4 electrolytes detected by the method of Watt and Chrisp after the 2 hours NRR test at corresponding potential.

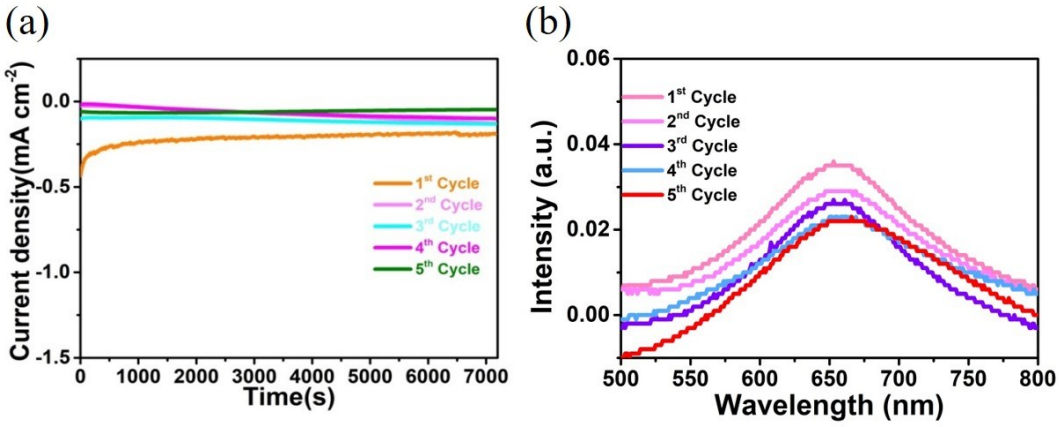

Figure S25. cycling test of $Ni_{0.75}Fe_{0.25}Se_2$. (a) Chrono-amperometry results of $Ni_{0.75}Fe_{0.25}Se_2$ at -0.1 V *vs*. RHE. (b) Corresponding UV-Vis absorption spectra of the electrolyte stained with indophenol indicator.

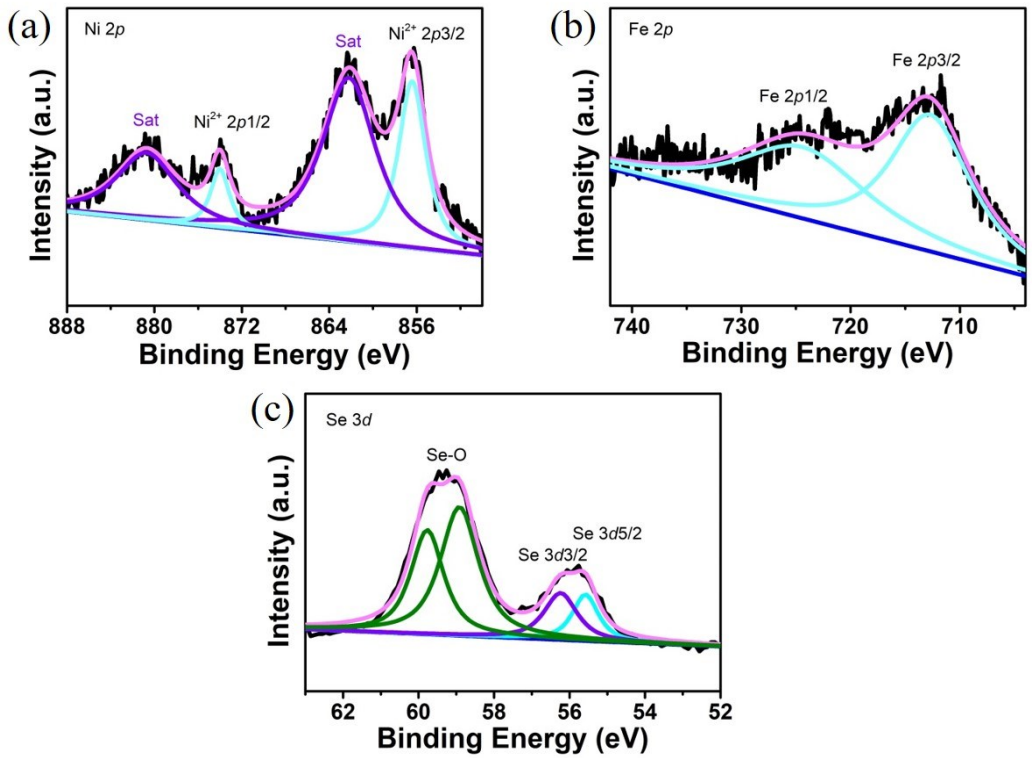

Figure S26. XPS spectra of $Ni_{0.75}Fe_{0.25}Se_2$ after the stability test (the 10-h N_2 reduction reaction). (a) Ni 2p; (b) Fe 2p; (c) Se 3d.

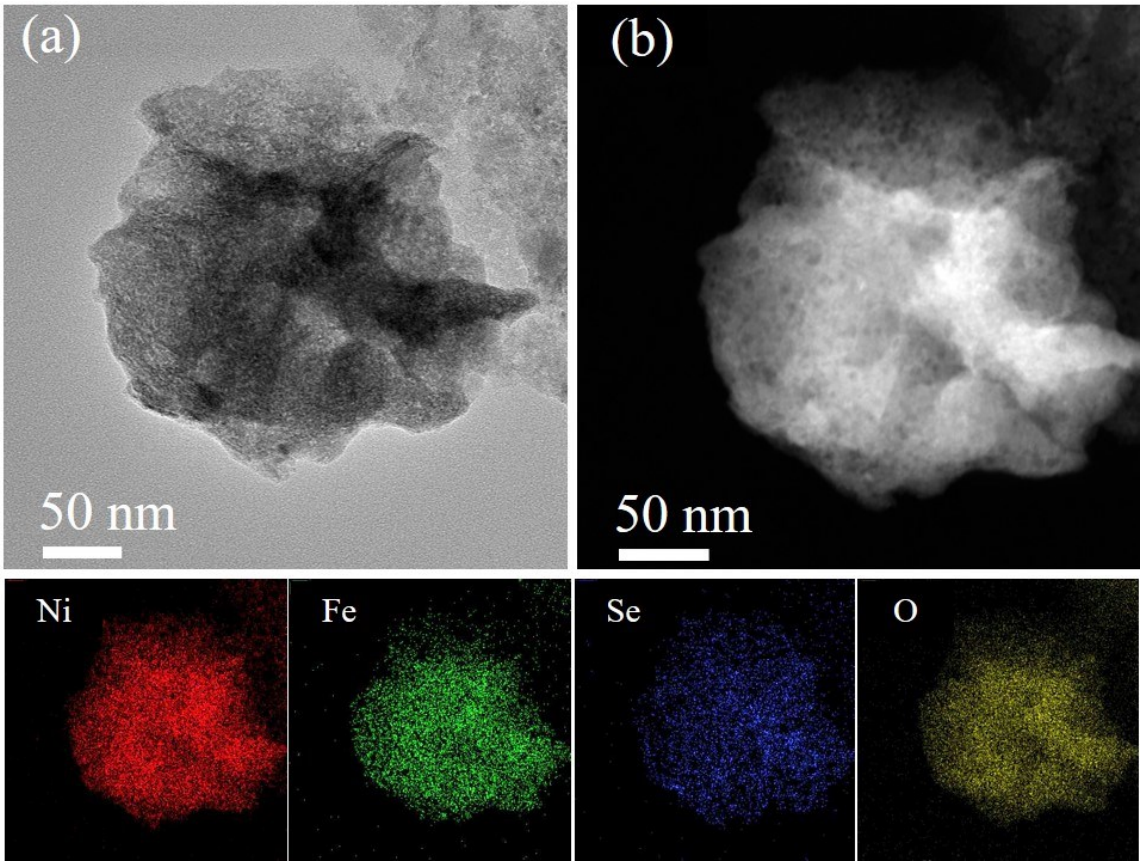

Figure S27. TEM image of $Ni_{0.75}Fe_{0.25}Se_2$ after the stability test. (a) TEM image of $Ni_{0.75}Fe_{0.25}Se_2$ after the 10-h N_2 reduction reaction. (b) EDS mappings of $Ni_{0.75}Fe_{0.25}Se_2$ after the 10-h N_2 reduction reaction for Ni (red), Fe (green), Se (purple) and O (golden).

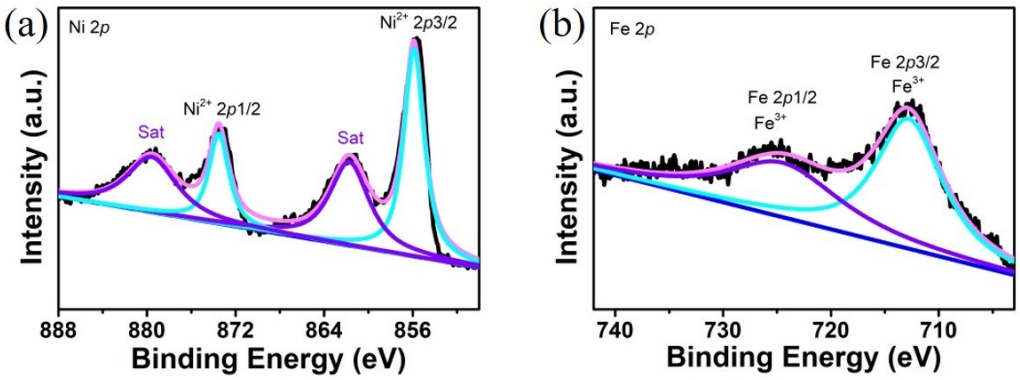

Figure S28. XPS spectra of $Ni_{0.75}Fe_{0.25}$-LDH. (a) Ni 2p; (b) Fe 2p.

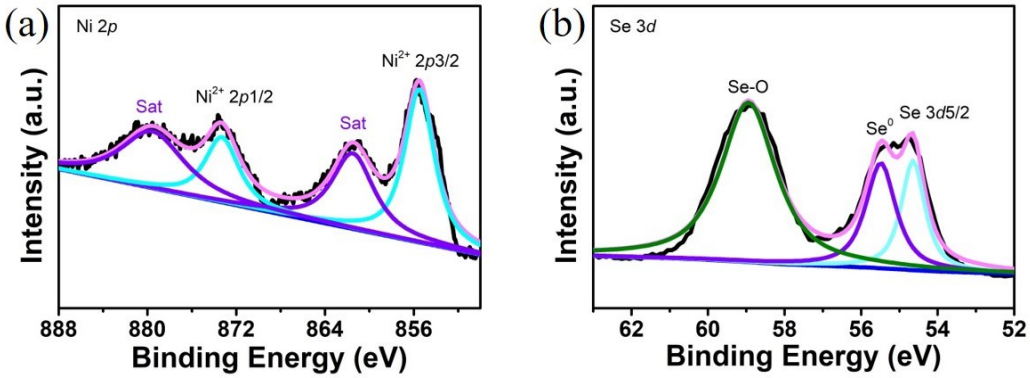

Figure S29. XPS spectra of $NiSe_2$. (a) Ni 2p; (b) Se 3d.

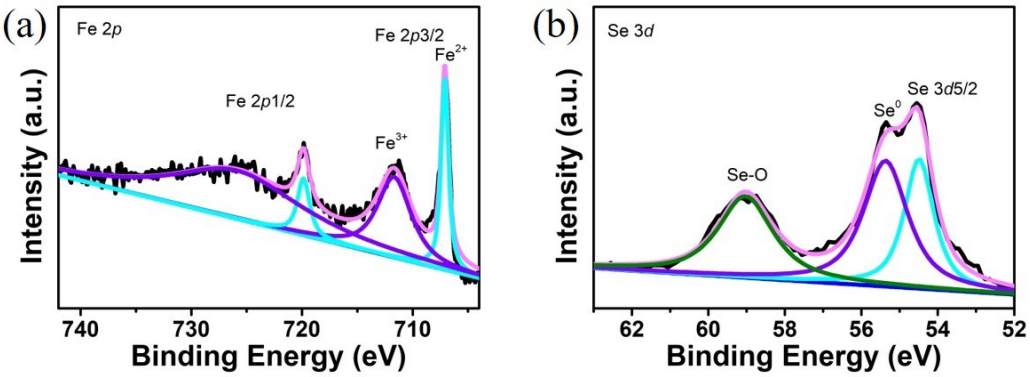

Figure S30. XPS spectra of $FeSe_2$. (a) Fe 2p; (b) Se 3d.

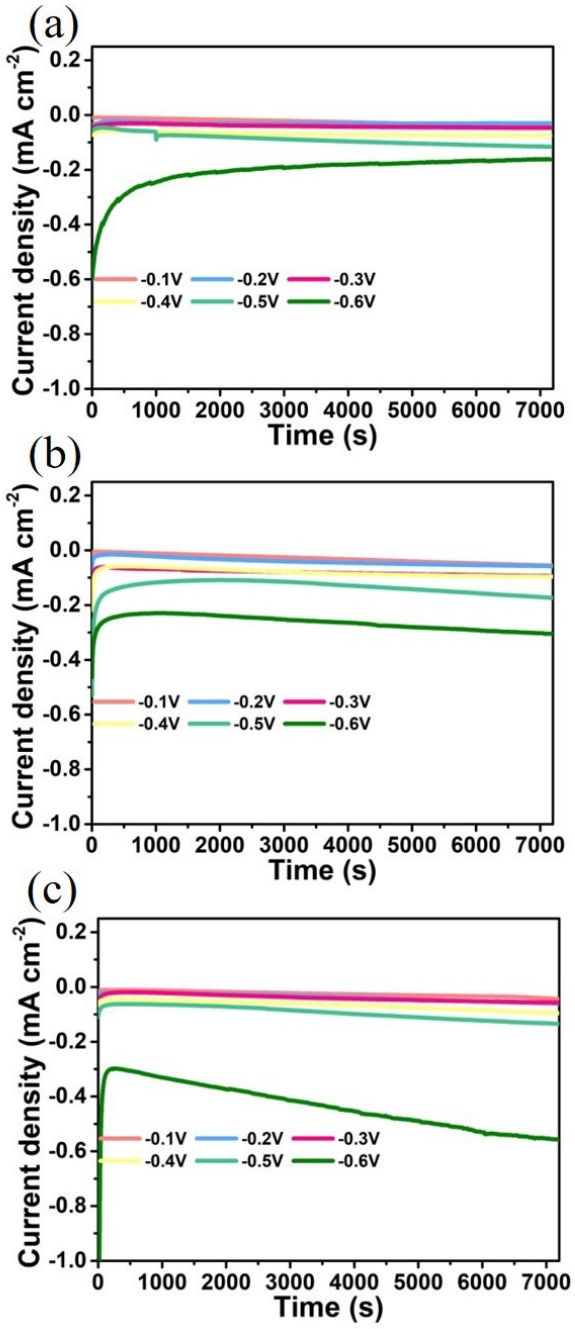

Figure S31. Chrono-amperometry results of (a) $Ni_{0.75}Fe_{0.25}$-LDH., (b) $NiSe_2$ and (c) $FeSe_2$ at the corresponding potentials, respectively.

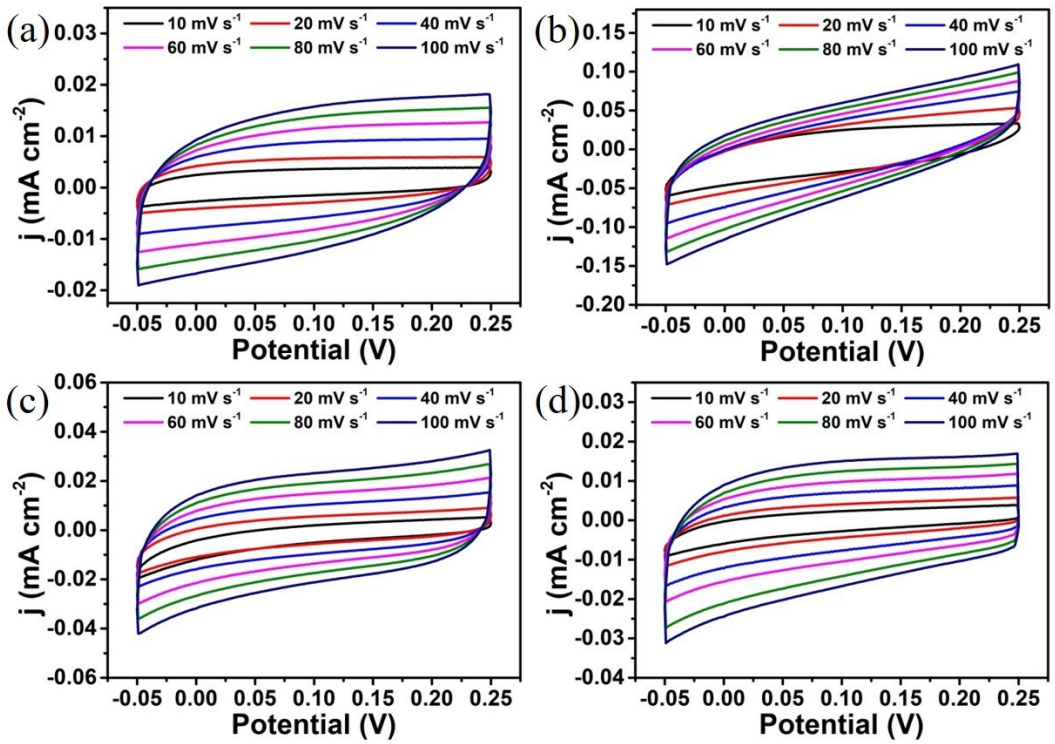

Figure S32. (a)-(d) Cyclic voltammograms for synthesized $Ni_{0.75}Fe_{0.25}$-LDH., $Ni_{0.75}Fe_{0.25}Se_2$, $NiSe_2$ and $FeSe_2$, respectively.

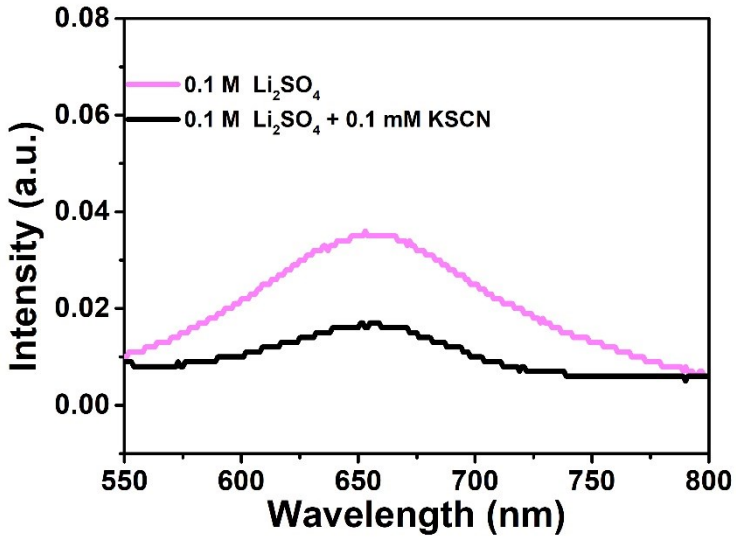

Figure S33. UV-Vis absorption spectra of the electrolyte of 0.1 M Li_2SO_4 and adding 0.1 mM KSCN stained with indophenol indicator at -0.1 V *vs*. RHE.

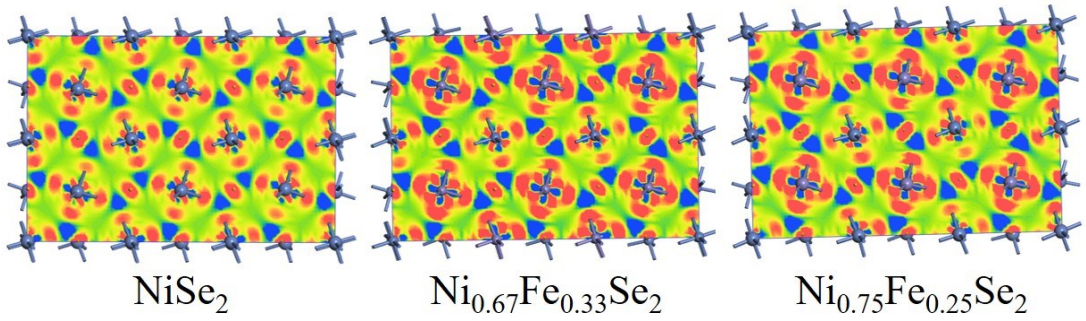

Figure S34. Charge density difference of $NiSe_2$; $Ni_{0.67}Fe_{0.33}Se_2$ and $Ni_{0.75}Fe_{0.25}Se_2$. In this plot a loss of electrons is indicated in blue, while electron enrichment is indicated in red.

Table S1. Calculated Ni/Fe ratio of NiFe-LDH from ICP-AES.

	Sample	Ni	Fe
Atom ratio	$Ni_{0.67}Fe_{0.33}$-LDH	2.06	1
	$Ni_{0.75}Fe_{0.25}$-LDH	3.09	1
	$Ni_{0.80}Fe_{0.20}$-LDH	3.93	1

Table S2. Calculated Ni/Fe ratio of NiFe-selenide from ICP-AES.

	Sample	Ni	Fe
Atom ratio	$Ni_{0.67}Fe_{0.33}Se_2$	2.13	1
	$Ni_{0.75}Fe_{0.25}Se_2$	3.04	1
	$Ni_{0.80}Fe_{0.20}Se_2$	3.86	1

Table S3. Summary of the representative noble metal catalysts and iron-based catalysts on electrocatalytic N_2 fixation.

Catalyst	Electrolyte	Yield rate	FE %	Testing method	Ref
Pt/C	phosphate buffer solution	4.5 μg h^{-1} mg^{-1}_{cat}	8.2	indophenol blue method	1
$Pd_{0.2}Cu_{0.8}$/rGO	0.1 M KOH	2.8μg h^{-1} mg^{-1}_{cat}	—	indophenol blue method	2
AuSAs-NDPCs	0.1 M HCl	2.32 μg h^{-1} mg^{-1}_{cat}	12.3	indophenol blue method	3
Ru/MoS_2	0.01 M HCl	1.14×10^{-10} mol s^{-1} cm^{-2}	17.6	indophenol blue method	4
THH Au NRs	0.1 M KOH	1.648 μg h^{-1} cm^{-2}	—	Nessler's reagent	5
Au HNCs	0.5 M $LiClO_4$	3.9 μg h^{-1} cm^{-2}	30.2	Nessler's reagent	6
Ag nanosheet	0.1 M HCl	4.62×10^{-11} mol s^{-1} cm^{-2}	4.8	indophenol blue method	7
Fe/Fe_3O_4	phosphate buffer solution	0.19 μg h^{-1} mg^{-1}_{cat}	8.29	indophenol blue method	8
FeSAs–N–C	0.1 M KOH	7.48 μg h^{-1} mg^{-1}_{cat}	56.55	indophenol blue method	9
FeSAs-MoS2	0.5 M K2SO4 (pH = 3)	8.63 μg h^{-1} mg^{-1}_{cat}	18.8	indophenol blue method	10

Ref.

1 J. Wang, L. Yu, L. Hu, G. Chen, H. Xin and X. Feng, Ambient ammonia synthesis via palladium-catalyzed electrohydrogenation of dinitrogen at low overpotential, *Nat. Commun.*, 2018, **9**, 1795.

2 M.-M. Shi, D. Bao, S.-J. Li, B.-R. Wulan, J.-M. Yan and Q. Jiang, Anchoring PdCu Amorphous Nanocluster on Graphene for Electrochemical Reduction of N_2 to NH_3 under Ambient Conditions in Aqueous Solution, *Adv. Energy Mater.*, 2018, **8**, 1800124.

3 Q. Qin, T. Heil, M. Antonietti and M. Oschatz, Single-Site Gold Catalysts on Hierarchical N-Doped Porous Noble Carbon for Enhanced Electrochemical Reduction of Nitrogen, *Small Methods*, 2018, **2**, 1800202.

4 B. H. R. Suryanto, D. Wang, L. M. Azofra, M. Harb, L. Cavallo, R. Jalili, D. R. G. Mitchell, M. Chatti and D. R. MacFarlane, MoS_2 Polymorphic Engineering Enhances Selectivity in the Electrochemical Reduction of Nitrogen to Ammonia, *ACS Energy Lett.*, 2018, **4**, 430.

5 D. Bao, Q. Zhang, F. L. Meng, H. X. Zhong, M. M. Shi, Y. Zhang, J. M. Yan, Q. Jiang and X. B. Zhang, Electrochemical Reduction of N_2 under Ambient Conditions for Artificial N_2 Fixation and Renewable Energy Storage Using N_2/NH_3 Cycle, *Adv. Mater.*, 2017, **29**, 1604799.

6 M. Nazemi, S. R. Panikkanvalappil and M. A. El-Sayed, Enhancing the rate of

electrochemical nitrogen reduction reaction for ammonia synthesis under ambient conditions using hollow gold nanocages, *Nano Energy*, 2018, **49**, 316.

7 H. Huang, L. Xia, X. Shi, A. M. Asiri and X. Sun, Ag nanosheets for efficient electrocatalytic N_2 fixation to NH_3 under ambient conditions, *Chem. Commun.*, 2018, **54**, 11427.

8 L. Hu, A. Khaniya, J. Wang, G. Chen, W. E. Kaden and X. Feng, Ambient electrochemical ammonia synthesis with high selectivity on Fe/Fe oxide catalyst, *ACS Catal.*, 2018, **8**, 9312.

9 M. Wang, S. Liu, T. Qian, J. Liu, J. Zhou, H. Ji, J. Xiong, J. Zhong and C. Yan, Over 56.55% Faradaic efficiency of ambient ammonia synthesis enabled by positively shifting the reaction potential, *Nat. Commun.*, 2019, **10**, 341.

10 H. Su, L. Chen, Y. Chen, Y. Wu, X. Wu, R. Si, W. Zhang, Z. Geng and J. Zeng, Single Atoms of Iron on MoS_2 Nanosheets for N_2 Electroreduction into Ammonia, *Angew. Chem., Int. Ed.*, 2020, DOI: 10.1002/anie.202009217.